JOURNAL OF MATERIALS SCIENCE 22 (1987) 4426–4433

The micromechanics of fatigue-induced delamination of a graphite/epoxy composite

W. L. MORRIS, A. K. ZUREK*
Rockwell International Science Center, Thousand Oaks, California 91360, USA

Fatigue crack growth in the resin layer between 0 and 90° plies of an AS/3501-5A graphite fibre/epoxy composite is discontinuous. Regularly spaced extensions of the crack front occur after periods of arrest. Crack compliance and tip strain fields have been measured to determine how the local minimum (K^{l}_{min}) and maximum (K^{l}_{max}) crack tip stress intensities affect growth. Contact of the fracture surfaces and swelling of the 90° ply modify these local stress intensities by an amount sensitive to load ratio (R), and the resulting propagation rate depends strongly on R. A model capable of describing this R effect relates the distance of each individual crack advance to K^{l}_{max} and the duration of each arrest to $K^{l}_{max} - K^{l}_{min}$, i.e., to ΔK_{eff}. We discuss the genesis of this model, and its explanation of the large Paris law coefficient which results if growth rates are instead expressed against the applied cyclic stress intensity.

1. Introduction

Sutton [1] reports that the Mode I fatigue crack growth rate in epoxy increases markedly with increased load ratio (R) up to $R = 0.7$. Furthermore, rates for Rs between 0.1 and 0.7 are superimposed when plotted against an energy release rate range, ΔG. This amounts to relating the growth rate to a product ($K_{mean}\Delta K$) of the applied mean and cyclic stress intensities. Contact of the fracture surface behind the crack front is a common source of such R effects in alloys [2–4]. But, its persistence in epoxy without saturating (i.e., without an R cutoff) to a 0.7 load ratio is unique, and cannot be justified by a contact mechanism alone. The large Paris law exponent found when the growth rate in epoxy and other organic resins is related to ΔK is also distinctive [5–7], and we see later a related phenomenon.

Epoxy is one of several resins in which discontinuous crack growth has been observed in fatigue [8, 9]. After each period of crack arrest, the front suddenly advances. Striations which mark each movement are reminiscent of stick-and-slip [10] behaviour common to sustained load growth. Lorenzo and Hahn [11] find that the separation between these marks, they identify as arrest lines, increases with crack length in a tensile epoxy specimen under constant cyclic load. So, the average crack front extension distance is clearly a factor in the fatigue growth rate. While the mechanics of the crack front movement in epoxy must still be established, in a PVC resin the distance of incremental crack advance and distance of crazing ahead of the crack front are monotonically related [12], suggesting a causal relationship. And, in a recent paper, Imai and Ward [13] make the plausible assumption in analysing fatigue crack growth rates in PMMA, that K_{max} (the maximum stress intensity) rather than ΔK controls the size of the craze. Their results are for fixed R, so the two variables are inseparable, but only a small liberty is needed to conclude that the discontinuous crack extension may actually be responding to K_{max}. For epoxy, the lack of a consensus about the presence of crazing during crack growth [14–17] clouds this logic. And, it would seem more likely that any growth phenomenon sensitive to an intensity maximum might find the local (K^{l}_{max}) rather than the applied (K_{max}) stress intensity more pertinent. Clearly, careful measurements of the local stress intensities at the crack tip against R ratio are needed to resolve the energetics of discontinuous crack advance. In this paper, we consider delamination of an epoxy matrix composite. It is subject to crack tip shielding, closure and residual stresses which can cause the local stress intensity to differ substantially from that deduced from the applied load.

We examine the delamination fatigue crack growth in an epoxy layer between 0 and 90° plies of Hercules AS/3501-5A – a path where discontinuous crack advance is pronounced. Stress intensity cannot normally be defined at a ply interface, but by finite element analysis of a similar laminate geometry, Wang [18] has found that a true $1/\sqrt{r}$ stress singularity is present between plies if there is an intervening resin layer. We use the strains measured in such a layer to estimate the local stress intensities, in order to validate more accurate values found by crack tip compliance measurements. Stereoscopic techniques [19] provided the strain field maps near the delamination crack tip needed to deduce K^{l}_{min}, K^{l}_{max} and the effective local stress intensity range $\Delta K_{eff} = K^{l}_{max} - K^{l}_{min}$. Data for two R ratios allow us to examine the structure spacing and duration of crack arrest in the laminate, in terms of these quantities.

* *Present address*: Los Alamos National Laboratory, MS-E546, Los Alamos, NM 87545, USA.

0022–2461/87 $03.00 + .12

2. Experimental details

The miniature fatigue machine illustrated in Fig. 1a was used to load a cantilever beam specimen (1) mounted on an optical microscope stage. Crack growth was followed and crack tip displacements were recorded by micrographs taken at ×250. A flow restrictor (2) regulated the rate of air pressure rise in the loading bellows, to control the loading rate, when the solenoid (3) in the three-way pressure valve (4) was electronically activated. The loading wave shape was trapezoidal, having a 5 Hz frequency and a loading rate of approximately 10^2 N sec^{-1}, and was read by a miniature load cell (5). The ambient temperature was 21° C.

Each cantilever beam specimen contained 50 plies of Hercules AS/3501-5A graphite/epoxy. The central two plies were of 90° orientation in an otherwise 0° laminate parallel to the crack propagation direction (Fig. 1b). The samples were cut from cured panels by a low-speed diamond saw and they were mechanically polished with alumina powder to remove surface damage. Crack growth was in plane strain and commonly in the resin layer between the 0° and 90° plies (Fig. 1c). The specimen mounting used prevented translation of the crack tip under applied load, simplifying the recording of optical micrographs used to find the crack tip strain fields. Strain field measurements described later show that, despite the constraint, the stress intensity was still largely Mode I. (The ratio of Modes II to I stress intensities was approximately 0.15 for the 50 ply specimen.)

To determine energy release rate and the applied K_I, a specimen compliance calibration was made in the conventional manner [20] by measuring (s) the deflection per unit load of the beam loading point against crack length (a). The strain energy release rate is simply

$$G = \frac{F^2}{2t}\left(\frac{ds}{da}\right) \quad (1)$$

where F is the applied force, and t is the specimen thickness. Values found for ds/da are given as a in Fig. 2. The equivalent K_I is $(GE_a)^{1/2}$, where E_a is Young's modulus of the 0° orientation specimen arms parallel to the crack.

The true minimum and maximum K_I at the crack tip differed somewhat from the intensities calculated using Equation 1. The disparity was only large when low growth rates exposed the laminate near the crack tip to substantial fatigue damage. In the analysis following, we consider only the predominantly Mode I component, and K_{min}, K_{max} and K^I_{min}, K^I_{max} refer to the applied and local Mode I stress intensities, respectively. For convenience, we also use the semantics of studies in alloys where the condition $K^I_{min} > K_{min}$ often results from contact of opposing surfaces behind the crack tip and is termed closure. This definition should only momentarily confuse the ceramist, for whom crack closure means $K^I_{max} < K_{max}$. Both types of "closure" are present in this delamination geometry as the result of local laminate swelling.

We found K^I_{min} and K^I_{max} from crack tip compliance

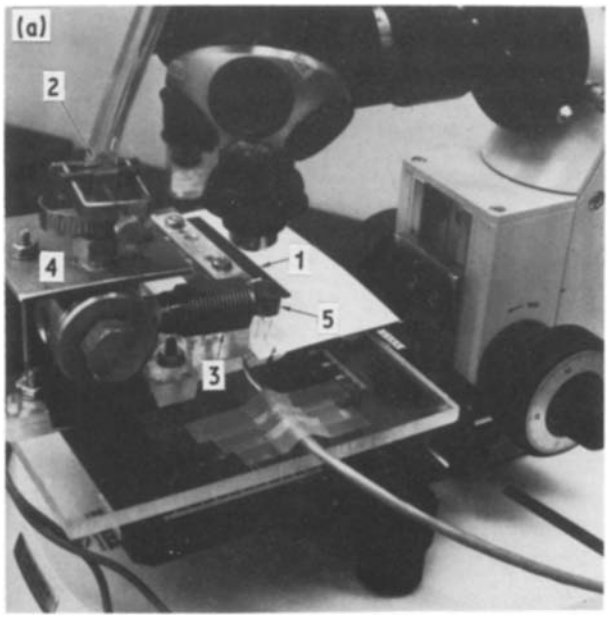

(b)

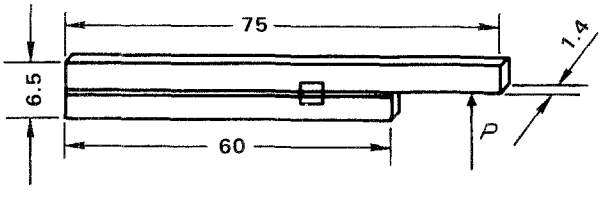

SPECIMEN DIMENSIONS [mm]

Figure 1 Specimen loading jig; (a) pneumatic loading frame mounted on an optical microscope stage; (b) cantilever beam specimen is loaded (P) as shown; (c) crack growth is characterized only when it follows its most natural path along the resin-rich layer (arrow) between the 0 and 90° plies.

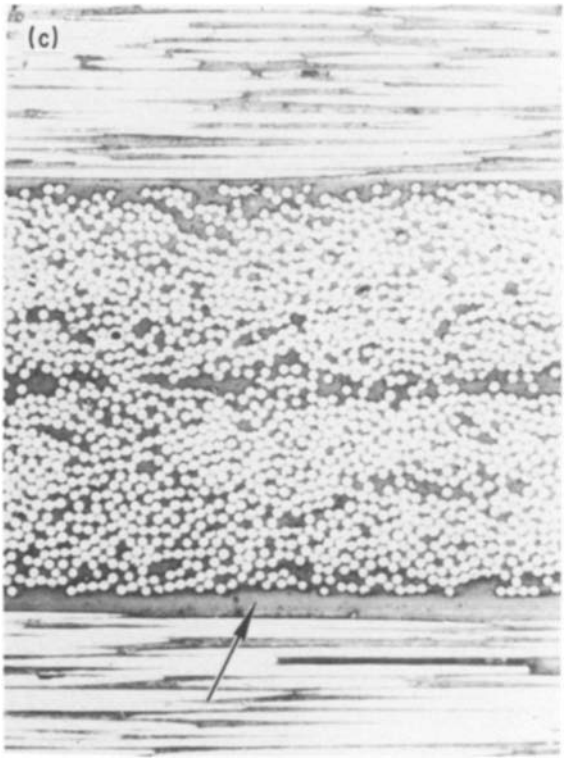

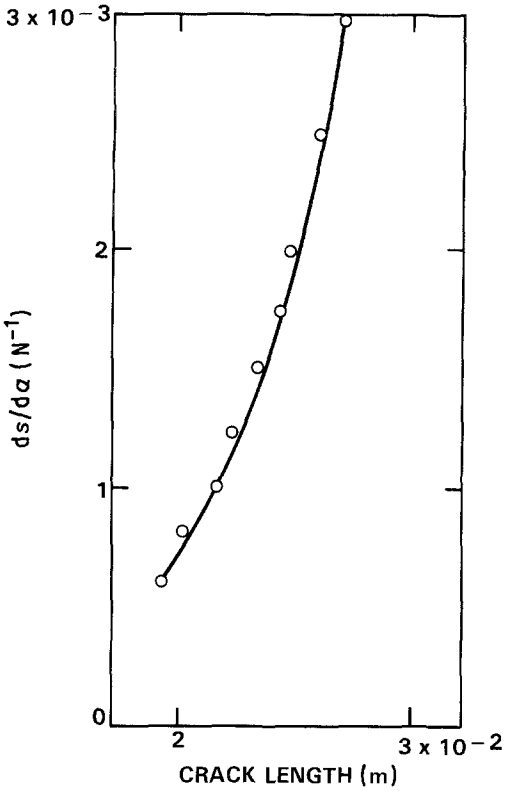

Figure 2 Compliance calibration curve for the cantilever specimen of Fig. 1b for 1.4 mm thickness.

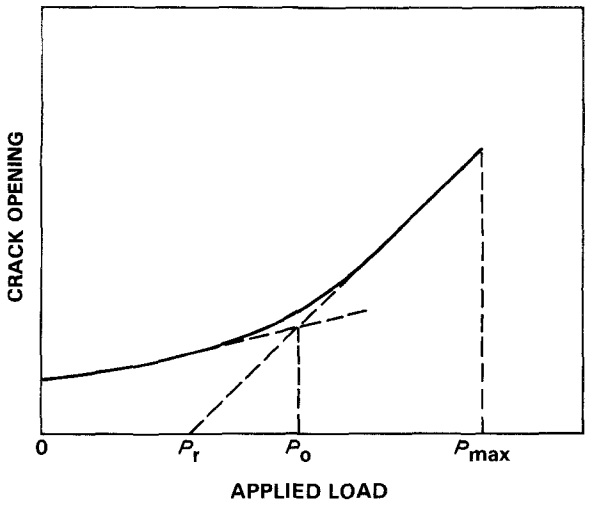

Figure 3 Schematic illustration of the method used to determine applied loads corresponding to the local values K^l_{min} and K^l_{max}. These are $(P_0 - P_r)$ and $(P_{max} - P_r)$, respectively. $P^l_{max} = P_{max} - P_r$ and $P^l_{min} = P_{max} - P_0$.

measurements, and also by a direct determination of the stress singularity magnitude in the resin layer just ahead of the crack tip. The latter is less a sensitive measurement, but is more direct. The local compliance data involve crack openings measured just behind (200 μm) the crack tip. There the crack opening displacement against applied load (P) was typically as illustrated in Fig. 3. The inflection at an external load P_0 is identified with the crack closure [21], and apparently results when contact of opposing fracture surfaces ceases for $P > P_0$. An estimate of the effective residual stress near the crack tip was also made, by extrapolating the elastic crack opening for $P > P_0$ to P_r at zero displacement as shown. P_r is approximately the external load at which the local stress at the crack tip would reach zero [22] if the crack could close fully, and therefore $(-P_r)$ is the load which cancels the local residual stress. The sum $(P_0 - P_r)$ is then the correct load to calculate K^l_{min}. K^l_{max} was found using $P_{max} - P_r$. ΔK_{eff} thus obtained equals $K^l_{max} - K^l_{min}$ and is the same as from the more conventional analysis of crack tip opening displacements in which P_r is ignored, and P_0 is defined as a closure load relative to a zero external load.

Values of K^l_{max} and K^l_{min} were also obtained by measuring the strains in the resin layer ahead of the crack tip. Wang [18] found that a $1/r^{1/2}$ stress singularity is identifiable in the intra-ply resin layer even for highly anisotropic lay-ups. Since the determination of local stress intensities from characteristics of the local crack opening against load is an art, it is comforting that the more direct measurement of stress intensity gives identical, albeit less accurate, values. Some simple manipulations of the crack tip displacement field equations of Irwin [23] allow us to relate the Modes I and II stress intensities to strains measured in the resin layer. The expressions are

$$K_I = \frac{2(2\pi)^{1/2} G_s x^{1/2}}{1 - 2\nu} \varepsilon_{yy} \quad (2)$$

$$K_{II} = \frac{2(2\pi)^{1/2} G_s x^{1/2}}{3 - 2\nu} \frac{dU_x}{dy} \quad (3)$$

where G_s is the resin shear modulus, ν is the Poisson's ratio, U is a displacement, and the strain $\varepsilon_{yy} = dU_y/dy$. The strain components given are for the x-axis in the growth direction and with the y-axis normal to the cracking plane. The maximum plastic zone size was about 2 μm, and all strains were measured outside this zone in the elastic resin layer. The local K_I calculated from strains measured at maximum external load is denoted K^l_{max}. At minimum external load, a non-zero residual value of K_I was observed, which resulted when the crack was held partially open by contacting fracture surfaces. This is K^l_{min}.

Displacement field maps from which ε_{yy} and dU_x/dy were found against x were obtained by stereoimaging [19]. Optical micrographs of the crack tip strains were made in pairs. One is a reference. To determine K^l_{min}, the reference must record the ply interface well ahead of a growing crack tip. A second micrograph is then made (at minimum load for K^l_{min}) after the crack tip arrives at the reference position. When the two micrographs are viewed as a stereoscopic pair in-plane displacements between the two, parallel to the axis of the stereoscope, stimulate visual differences in surface height. These are converted to the corresponding linear displacements by a travelling spot analysis [24]. The one-dimensional components of the displacement over a two-dimensional grid are then used to define locations of constant local strain fields. The advantage of stereoscopic analysis is measurement sensitivity. We achieved absolute displacement accuracies of $\pm 5\,\mu$m from optical micrographs, corresponding to strain sensitivities of $\pm 2 \times 10^{-3}$ over a 10 μm gauge length on the specimen surface. This amounts to sensing shifts in the diffraction edge of identical high

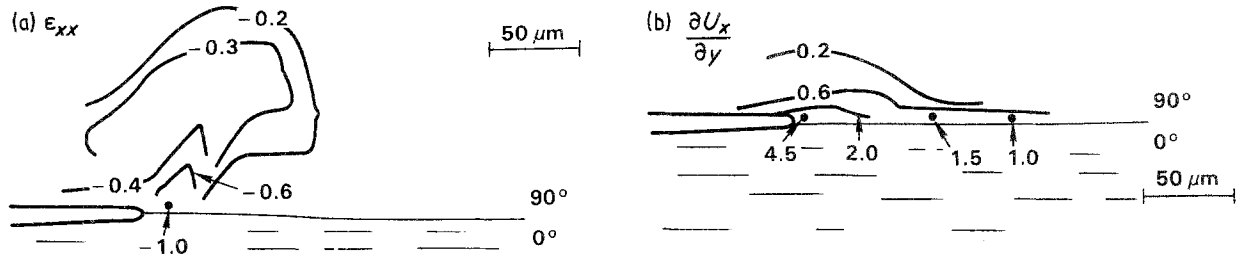

Figure 4 Example iso-strain contours of total strain near delamination crack tip, showing (a) the ε_{xx} tensile component normal to the crack tip; (b) and the $\partial u_x/\partial y$ component of the shear strain parallel to the delamination interface. Results are total strain at maximum load measured relative to the uncracked interface.

contrast objects in the two images with an accuracy of 1/10 of the width of an edge diffraction profile.

Since optical micrographs were used, extreme care was needed to avoid strain errors from distortion of the optical image due to nonlinearities in the microscope optics. Each pair of micrographs was recorded of essentially identical areas along the ply interface, and a through focus series was occasionally used to obtain a second micrograph best matching the reference image. An important advantage of using optical images, which made this effort worthwhile, is the high stability of optical magnification. This allowed the reference micrograph to be recorded hours before the second micrograph, which imaged the propagated crack tip, was secured.

The iso-strain-contour maps in Fig. 4 result from this procedure and can be used to find both K_I (Fig. 4a) and K_{II} (Fig. 4b) using Equations 2 and 3. In the example analysis in Fig. 5, Mode II strains along the interface were found at a maximum load and high growth rate. In this case, there is little fatigue damage to the laminate around the crack tip, $K^I_{max} \sim K_{max}$, and the maximum K_{II} scales, as expected, with the square root of the energy release rate calculated by Equation 1.

As another test of the consistency of these various measurements, the shear modulus of the resin layer at the crack tip was calculated by solving Equation 2 for G_s and inserting experimentally measured ε_{yy} against x. For an assumed value of $\nu = 0.3$, this gave $G_s = 1.16$ GPa for the resin, about 20% smaller than the bulk value. K_I found using Equation 2 is within $\pm 20\%$ of that calculated from energy release rate, if the growth rate is high and there is little ply swelling.

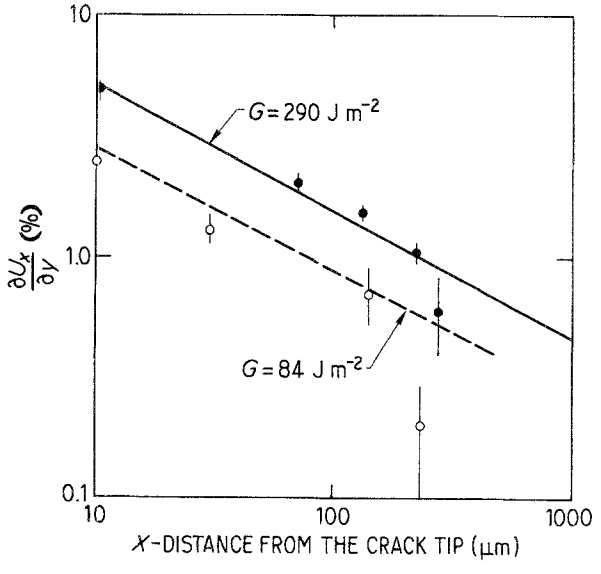

Figure 5 Example analysis of $\partial u_x/\partial y$ against distance x from the crack tip. Used in this case to determine the magnitude of the Mode II stress intensity. Results scale as expected with energy release rates. The dashed line for 84 J m^{-2} is predicted from the strains found for 290 J m^{-2}. K_{II} is approximately 15% of K_I.

3. Growth observations

Fatigue striations were observed on most of each specimen's fracture surface, and apparently demark sites of crack arrest (Fig. 6). Their spacings were large compared to the average cycle-by-cycle growth distance, so the propagation presumably involved sudden advances of a periodically arrested crack front. Precisely such jumps of the crack tip were seen in the propagation rate and the associated periods of arrest observed are consistent with the average growth rate and the measured striation spacings. By infiltration of the crack and sectioning we established that a striation indeed marks the position of true crack front. But, the structures are present only if the intra-ply resin layer is sufficiently thick, in excess of several micrometers, and so may just be useful artifacts *indicative* of rather than *the structure which* caused the arrest. A typical cross-section of a striation is as illustrated schematically in Fig. 6c. The crack front usually passed along the 90° ply, primarily at the fibre/matrix interface. Individual lines were actually ridges of resin, left behind on the 90° fibres at intervals. On perhaps 10% of the fracture surface this pattern was reversed, and the 0° fibres were cleaned of resin, with only the periodic resin ridges remaining. A clue to the mechanism of the striation formation is that they were also present during sustained fast fracture at K_{Ic}. So they are related to stick–slip markings [10, 25] more normally seen in sustained load tests. However, we found no propagation along the ply interface under sustained constant load – only with cyclic loading. The fatigue-induced striations were regularly spaced, and their separation increased approximately quadratically with K_{max}, as apparent in Fig. 7. However, data for two R ratios show that K_{max} alone does not precisely determine the striation spacing.

Crack growth rates along the 90°/0° interface and their response to R are shown in Fig. 8. The crack front advanced in increments and at the surface the discontinuous growth rate increased with the local angle of the crack front relative to the surface. The crack tunnelled ahead a bit in the specimen centre, so that at low growth rates the typical crack front reached

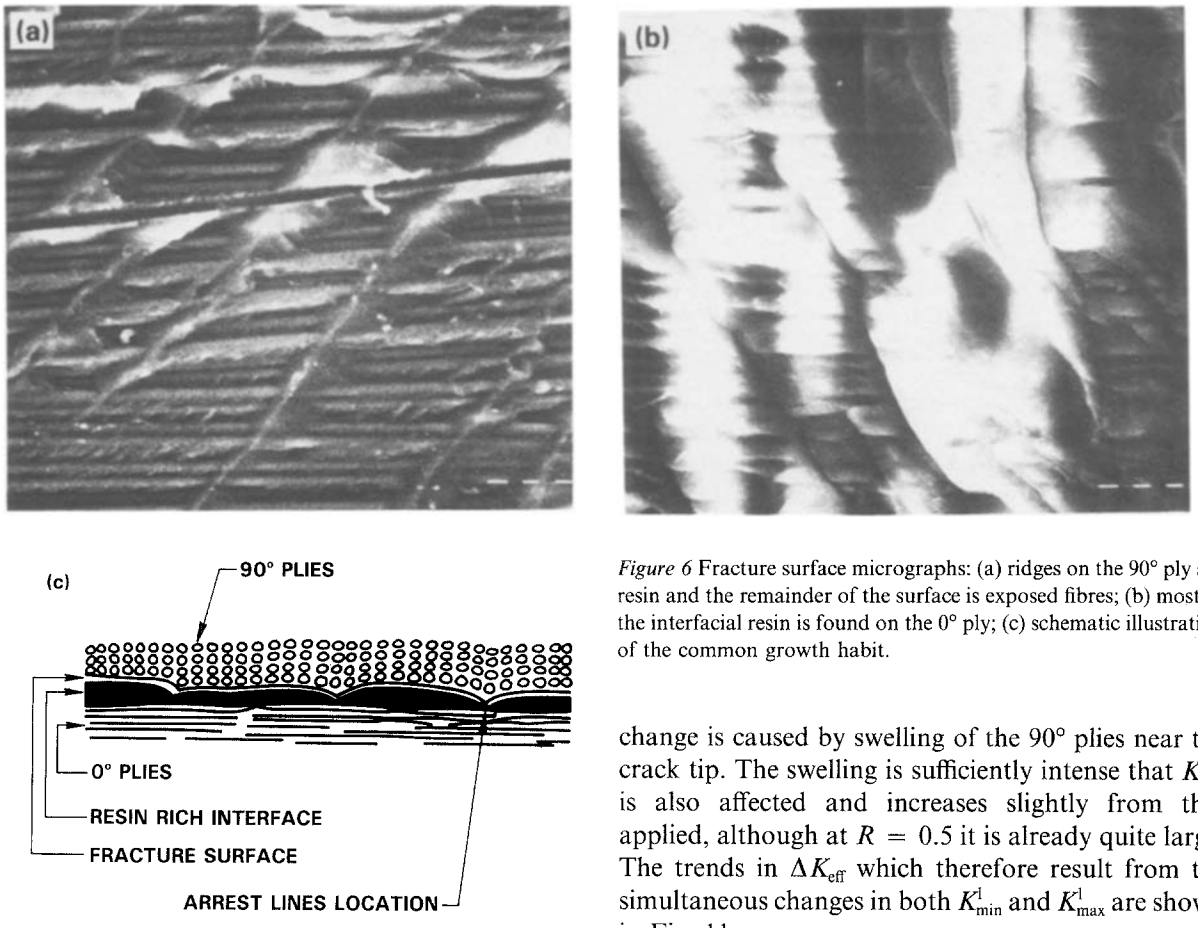

Figure 6 Fracture surface micrographs: (a) ridges on the 90° ply are resin and the remainder of the surface is exposed fibres; (b) most of the interfacial resin is found on the 0° ply; (c) schematic illustration of the common growth habit.

the surface rotated about 35° from the propagation direction. A substantial variation was found in this angle, and this variability must be a factor in the large scatter in growth rate apparent in Fig. 8.

Values found for the local minimum (K^1_{min}) and maximum (K^1_{max}) stress intensities at a propagating crack tip are given against K_{max} in Figs 9 and 10 for $R = 0$ and $R = 0.5$, respectively. These were determined by analysis of crack-opening displacement (solid circles), and by measuring the local stress intensity directly (open circles). An especially dramatic drop occurred in K^1_{max} at $R = 0.5$ and low growth rates. Strain field measurements suggest to us that this change is caused by swelling of the 90° plies near the crack tip. The swelling is sufficiently intense that K^1_{min} is also affected and increases slightly from that applied, although at $R = 0.5$ it is already quite large. The trends in ΔK_{eff} which therefore result from the simultaneous changes in both K^1_{min} and K^1_{max} are shown in Fig. 11.

4. Discussion

High resolution strain field maps made by scanning electron microscopy ahead of a newly arrested crack tip and around individual 90° ply fibres revealed that fatigue produces localized flow in the epoxy at the fibre/resin interface. With persistent fatigue, each interface near the ply interface microcracked. A plane

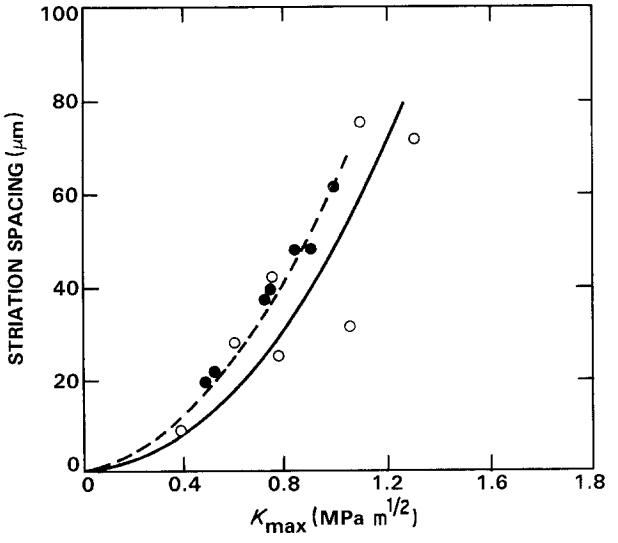

Figure 7 Growth striation spacing against K_{max}. Curve are of the form $r_j \propto K^2_{max}$. (●) $R = 0.5$, (○) $R = 0$.

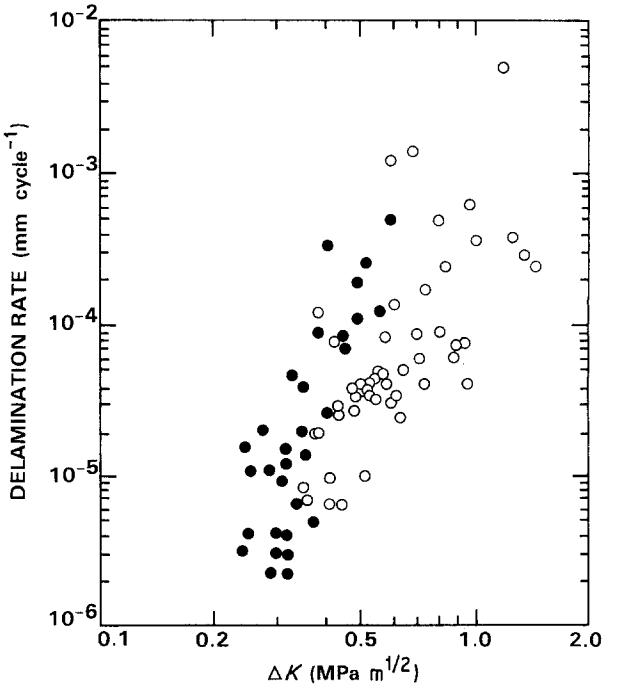

Figure 8 Delamination growth rates against ΔK. (●) $R = 0.5$, (○) $R = 0$.

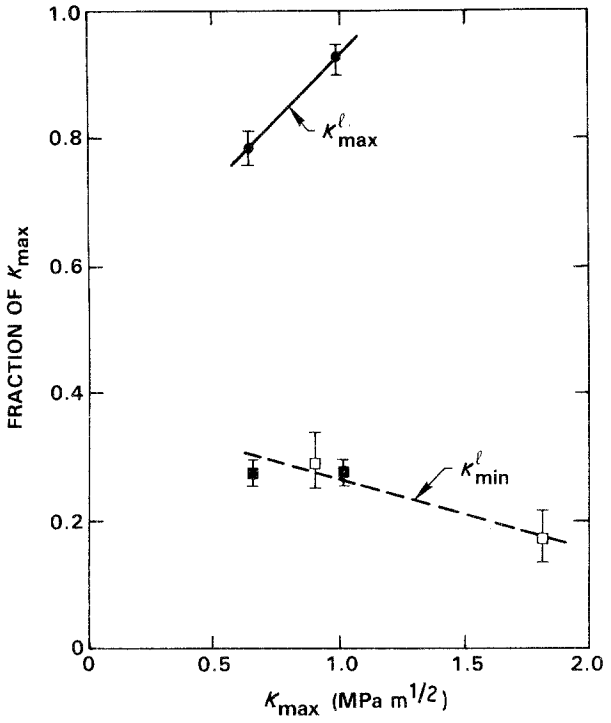

Figure 9 Local K^{l}_{min} and K^{l}_{max} against applied K_{max} for $R = 0$. Solid circles are from $x^{-1/2}$ measurements, and open circles from crack opening against load.

containing fibre/matrix interface microcracks ultimately extended ahead of the main crack tip near the 90° ply/resin layer interface. Discontinuous growth through this zone produces striations separated by a distance $r_j(K_{max})$ as per Fig. 7. A possible explanation, we now reject, for the apparent relationship of r_j to K_{max} is that each jump distance was limited by the size of the microcracked process zone. One would then anticipate $r_j \propto (K_{max})^2$, in rough agreement with observation. But, there are several problems with this idea. At the surface r_j is much smaller than the distance of microcracking we observed ahead of the

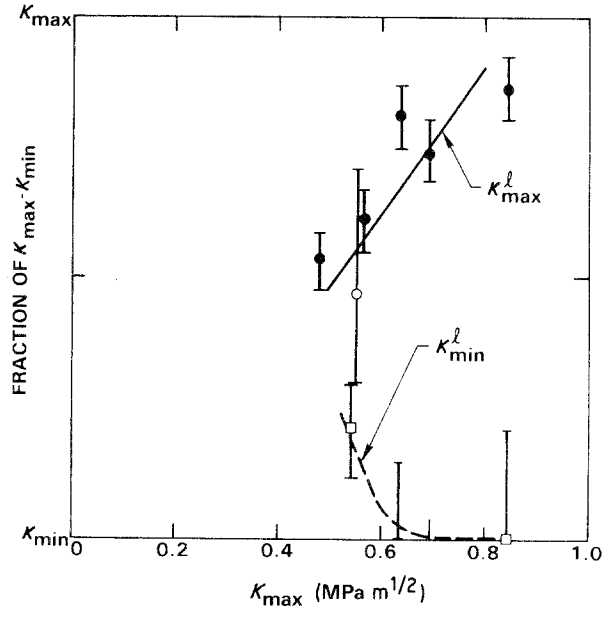

Figure 10 Local K^{l}_{min} and K^{l}_{max} against K_{max} for $R = 0.5$. Solid circles are from $x^{-1/2}$ measurements, and open circles from crack opening against load.

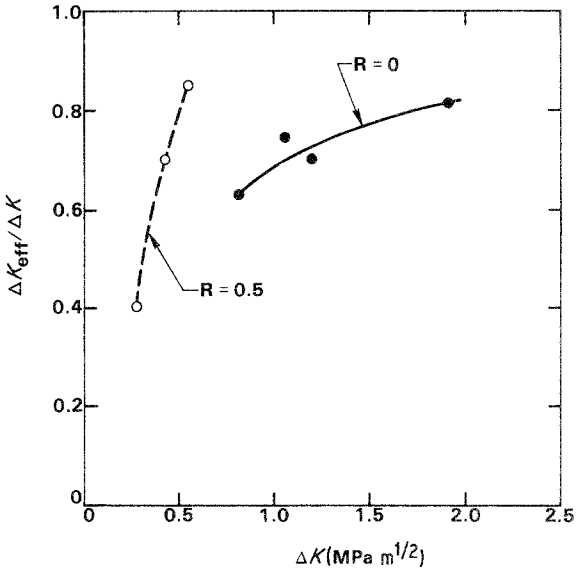

Figure 11 Effective stress intensity values against ΔK. (●) $R = 0.5$, (○) $R = 0$.

crack tip. Also, such a process zone size restriction on r_j neither explains why the striations persist during critical propagation, nor why the arrest line spacing is unchanged if the cracking path is along the 0° rather than the 90° fibres.

Lorenzo and Hahn's [11] identification of striations in pure epoxy as arrest lines suggests another possibility. Fatigue ultimately promotes crack movement through the process zone at a K_{max} less than K_{Ic} of the undamaged laminate, until arrest occurs. The increment of crack extension will increase monotonically with K_{max}, and only the functional form for r_j must be found. Since the distance of each crack advance may also depend on the degree of fatigue damage ahead of the crack tip, a sensitivity of r_j to R as well as to K_{max} can be anticipated. Actually, however, it is more likely that any influence of maximum stress intensity on r_j would rather be local, hence K^{l}_{max}. We can use the observed average K^{l}_{min} and K^{l}_{max} values against K_{max} to determine if the local stress intensities better describe the R behaviour.

In Fig. 12 we compare r_j to ΔK_{eff} (Fig. 12a) and to K^{l}_{max} (Fig. 12b), by using the results of Figs 9 and 10 to redefine the abscissa of Fig. 6. Only K^{l}_{max} correlates the results for the two R ratios. Some residual R dependence remains, but a K^{l}_{max} description of r_j makes a slight improvement over that by K_{max} in Fig. 7. Also, clearly $r_j \propto (K^{l}_{max})^2$ is not correct, although it suffices to represent the data if behaviour at both small and large K^{l}_{max} must be described.

To find the average duration of each crack arrest (n_a), for the two R ratios, we divided the average striation spacing by the average growth rate against R and use the data of Figs 9 and 10 to relate n_a to ΔK_{eff} (Fig. 13a) and to K^{l}_{max} (Fig. 13b). The strongest correlation is then of n_a with ΔK_{eff}. The approximate inverse quadratic relationship to ΔK_{eff} is consistent with a fatigue damage mechanism as the controlling process in the duration of crack arrest [26].

To write an expression for the average growth rate let us assume that the discontinuous growth involves

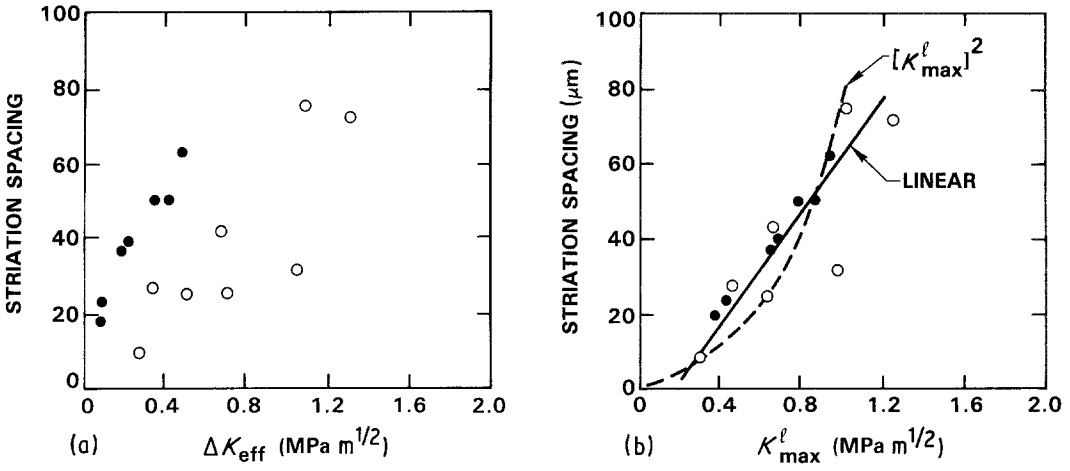

Figure 12 Striation spacing against (a) ΔK_{eff}; (b) K^{l}_{max}. (●) $R = 0.5$, (○) $R = 0$.

an incremental crack advance $r_j \propto (K^{l}_{max})^2$ and an arrest duration $n_a \propto (\Delta K_{eff})^{-2}$. Imagine that a small zone, perhaps of fixed size l_0, must be crossed at each arrest site before the next increment of growth. The growth rate through this zone will be $\Delta l_0/\Delta N \propto \Delta K^2_{eff}$, so that

$$n_a \propto (\Delta K_{eff})^{-2} l_0 \tag{5}$$

The growth rate averaged over l_0 and r_j then becomes

$$\overline{\frac{da}{dN}} = \frac{r_j}{n_a} = A(K^{l}_{max})^2 \Delta K^2_{eff} \tag{6}$$

if $l_0 \ll r_j$, where (A) is a material parameter. By construction we know that for a single R ratio the agreement of Equation 6 with experiment will be good. But, the reasonable description Equation 6 provides for the averaged growth rate data for a second R ratio in Fig. 14 suggests that the underlying growth mechanics may have been correctly described. In contrast, the Paris law representation of the raw rate data of Fig. 8 is

$$\frac{da}{dN} \propto \Delta K^{5.6} \tag{7}$$

but the rates depend upon the R ratio. Equation 6 tells us that the very large 5.6 exponent is actually the result of an ancillary dependence of the growth on K^{l}_{max}. Equation 6 is very similar in form to the expression arrived at empirical by Sutton for epoxy some years ago. The equation has other attributes, which should be tested in the future. For example, substantial acceleration in average growth rate by infrequent overloads might result, if individual overloads could extend the front by l_0. Then the total crack would presumably advance a distance r_j for each overload.

Marshall *et al.* [27] have determined, in modelling of transformation toughening of ceramics, that K^{l}_{max} is reduced only by expansion of material behind the crack tip. Indeed we observe such swelling by strain field mapping. It is present in the 90° ply both ahead of and behind the crack tip at growth rates below 10^{-6} mm cycle^{-1}, and probably causes the change in K^{l}_{max} which contributes to the rapid acceleration in growth rate as K^{l}_{max}/K_{max} increases with K_{max}. Compressive strains in the resin exceeding 0.5% in the y direction were found near a slowly moving crack tip. One thought is that the swelling may result from microcracking of fibre/matrix interfaces in the 90° plies. Moisture-induced swelling of the resin could also explain the result, but must be fatigue assisted. A decrease in K^{l}_{max} is also consistent with strain-induced toughening of the resin stemming from preferential alignment of the polymer molecules, as discussed by Berry [28]. Swelling of the 90° ply apparently acts to self-perpetuate low growth rates, in that the slower the

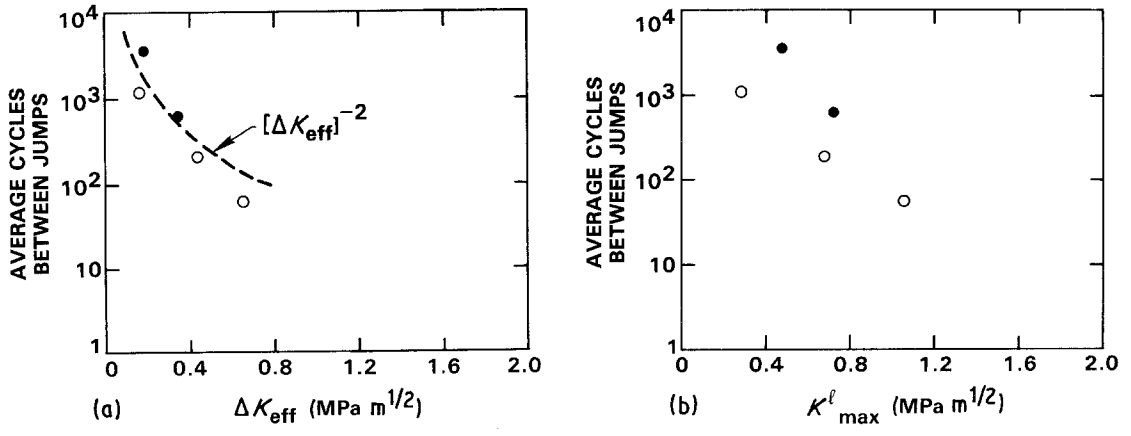

Figure 13 Average crack arrest duration against (a) ΔK_{eff}; (b) K^{l}_{max}, calculated from r_j and average growth rate for each load ratio. (●) $R = 0.5$, (○) $R = 0$.

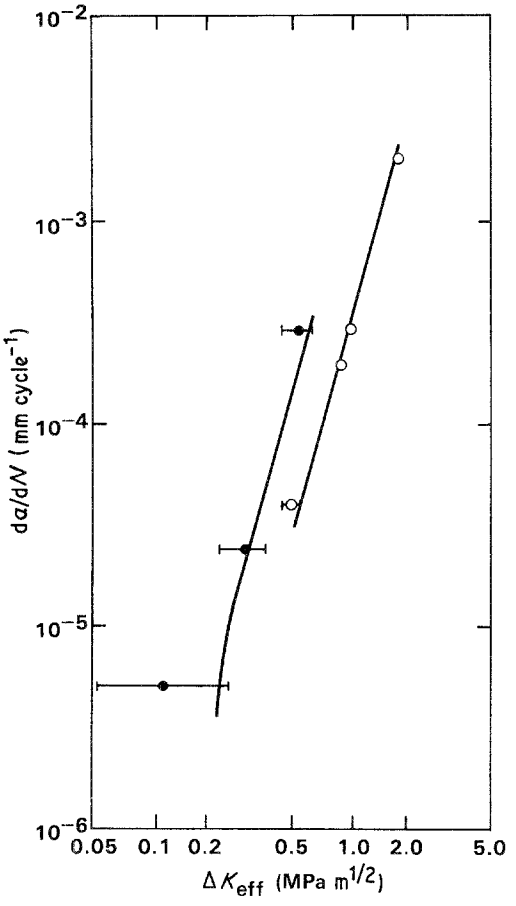

Figure 14 Comparison of averaged growth rates and predictions of Equation 6. (●) $R = 0.5$, (○) $R = 0$.

crack front moves the more damage, swelling, and hence reduction in K^{l}_{max} occurs. The propagation rate in such a system may not even reach true equilibrium at constant K_{max}. It is amazing that a conventional energy release rate or linear elastic fracture mechanics analysis of growth rate has any utility in such a material.

5. Summary

Delamination fatigue crack growth between the 0° and 90° plies of AS/3501-5A has been characterized. It has aspects which resemble both the K^{l}_{max} sensitivity of brittle cracking in ceramics and the ΔK_{eff} sensitivity of fatigue propagation in alloys. The propagation in the Gr/Ep laminate is discontinuous with periodic arrests made apparent by arrest lines. A study of the spacing of these features for two load ratios shows that the distance of each crack advance is controlled by K^{l}_{max}. The duration of the intervening crack arrests is related to ΔK_{eff}. The actual crack movement during the fatigue sensitive phase is too small to measure. So, the average propagation rates involve a mixture of subcritical crack advance and fatigue driven changes to the crack tip properties. Perhaps, the latter lowers the local toughness, allowing the next increment of crack movement. The resulting growth rates depend strongly on the local minimum and maximum stress intensities, and the precipitous increase in growth rate, as ΔK is raised, is apparently largely the result of the discontinuous propagation and the coupling of the distance of incremental crack advance to K^{l}_{max}.

Acknowledgements

This research was supported by Rockwell International IR&D funds. The assistance of R. V. Inman in collecting the growth rate data is greatly appreciated.

References

1. S. A. SUTTON, *Eng. Frac. Mech.* **6** (1976) 587.
2. H. L. MARCUS, W. L. MORRIS, O. BUCK and J. D. FRANDSEN, "Prospects of Fracture Mechanics", edited by G. C. Sih, H. C. van Elst and D. Broek (Nordhoff International Publishers, 1974) p. 197.
3. S. SURESH, G. F. ZANISKI and R. O. RITCHIE, *Met. Trans.* **12A** (1981) 1435.
4. P. K. LIAW, T. R. LEAX, R. S. WILLIAMS and M. G. BECK, *ibid.* **13A** (1982) 1607.
5. A. M. SERRANO, G. E. WELSCH and R. GIBOLA, *Poly. Eng. Sci.* **15** (1982) 946.
6. T. M. WRIGHT and R. P. ROBINSON, *J. Mater. Sci.* **17** (1982) 2463.
7. T. A. MORELLI and M. T. TAKEMORI, *ibid.* **19** (1984) 385.
8. A. CHADNOVSKY and A. MOET, *Poly. Eng. Sci.* **15** (1982) 922.
9. M. T. TAKEMORI, *Poly. Eng. Sci.* **15** (1982) 937.
10. D. C. PHILLIPS, J. M. SCOTT and M. JONES, *J. Mater. Sci.* **13** (1978) 311.
11. L. LORENZO and H. T. HAHN, *Poly. Eng. Sci.* **16** (1986) 274.
12. L. KONIZOL, M. G. SCHINKER and W. DOLL, *J. Mater. Sci.* **19** (1984) 1605.
13. Y. IMAI and I. M. WARD, *ibid.* **20** (1985) 3842.
14. S. YAMINI and R. J. YOUNG, *ibid.* **15** (1980) 1823.
15. A. J. KINLOCH, S. J. SHAW, D. A. TOD and D. L. HUNSTON, *Polymer* **24** (1983) 1341.
16. R. J. MORGAN, E. T. MONES and W. J. STEELE, *ibid.* **23** (1982) 295.
17. S. YAMINI and R. J. YOUNG, *J. Mater. Sci.* **15** (1980) 1814.
18. S. S. WANG, "Composite Materials: Testing and Design", ASTM STP 674, edited by S. W. Tsai, (ASTM, 1979) p. 642.
19. D. P. WILLIAMS, D. L. DAVIDSON and J. LANKFORD, *Exp. Mech.* **20** (1980) 134.
20. B. A. LAWN and T. R. WILSHAW, "Fracture of Brittle Solids" (Cambridge University Press, Cambridge, 1975) p. 49.
21. W. L. MORRIS, M. R. JAMES and O. BUCK, *Met. Trans.* **12A** (1981) 57.
22. W. MORRIS and M. R. JAMES, "Fatigue Crack Growth Threshold Concepts", edited by D. L. Davidson and S. Suresh (AIME, Warrendale, 1984) p. 479.
23. G. R. IRWIN, *J. Appl. Mech.* **79** (1957) 361.
24. W. L. MORRIS, R. V. INMAN and M. R. JAMES, *J. Mater. Sci.* **17** (1982) 1413.
25. A. J. KINLOCK and J. G. WILLIAMS, *ibid.* **15** (1980) 987.
26. A. K. ZUREK, M. R. JAMES and W. L. MORRIS, *Met. Trans.* **14A** (1983) 1697.
27. D. B. MARSHALL, A. G. EVANS and M. DRURY, "Fracture Mechanics of Ceramics 6", edited by R. C. Bradt, A. G. Evans, D. P. H. Hasselman and F. F. Lange (Plenum, 1983) p. 289.
28. J. T. BERRY, "Fracture Processes in Polymeric Solids", edited by B. Rosen (John Wiley and Sons, 1967) p. 195.

Received 17 February
and accepted 28 April 1987